buildings

MDPI

Article

Welding Residual Stress Elimination Technique in the Top Chord of Main Truss of Steel Truss Bridge

Long Piao [1,2], Jianfeng Yuan [3], Niujing Ma [1,*], Changqi Yue [1], Ronghui Wang [1] and Gangbing Zheng [4]

1 School of Civil Engineering and Transportation, South China University of Technology, Guangzhou 510640, China; piaolong20230321@163.com (L.P.); 202221009036@mail.scut.edu.cn (C.Y.); rhwang@scut.edu.cn (R.W.)
2 Guangdong East Guangdong Intercity Railway Co., Ltd., Guangzhou 510640, China
3 Hangzhou Olympic Sports Expo Center Xiaoshan Construction Investment Co., Ltd., Hangzhou 311215, China; m15967185274@163.com
4 Hangzhou Huaxin Testing Technology Co., Ltd., Hangzhou 311215, China; zyt18967170808@163.com
* Correspondence: ctmaniujing@scut.edu.cn; Tel.: +86-186-6600-1881

Abstract: The large-amplitude fluctuations of ultrasound in high-energy ultrasonic stress relieving cause the crystal grains or lattices in the high residual stress zone to vibrate or creep alternately. This triggers secondary effects such as ultrasonic softening and dislocation movement. The sound field also produces periodic shock waves or intermittent shock waves, which form local pressure gradients at the wave front. These pressure gradients cause local heating of the grain boundary, accelerating material softening and promoting slip between grains, ultimately resulting in residual stress elimination. This technique was applied to detect the welding residual stress of the upper chord of the main truss of Sanguantang Bridge by using an ultrasonic stress meter. After the measurement, it was found that the welding residual stress in some areas was too large, and the welding residual stress needed to be eliminated. The welding seam was re-inspected after the residual stress relief operation was completed. The test results showed a maximum reduction rate of 63.91% and an average overall reduction rate ranging from 24.52% to 37.23%. The reduction effect is more significant in areas with higher welding residual stress.

Keywords: steel truss bridge; welding residual stress; axial force testing; ultrasonic measurement; high-strength bolts

Citation: Piao, L.; Yuan, J.; Ma, N.; Yue, C.; Wang, R.; Zheng, G. Welding Residual Stress Elimination Technique in the Top Chord of Main Truss of Steel Truss Bridge. *Buildings* **2023**, *13*, 1267. https://doi.org/10.3390/buildings13051267

Academic Editors: Yonghui Huang, Zhicheng Yang and Zhou Chen

Received: 14 April 2023
Revised: 4 May 2023
Accepted: 11 May 2023
Published: 12 May 2023

1. Introduction

In the welding process of steel structures, a partial zone is subjected to a high temperature, which causes uneven heating and cooling, resulting in welding deformation of the components. High quantities of welding produce complex welding residual stress, which mainly exists in the welding seam, and will reduce the proportional limit of the steel before yielding. At the same time, the residual stress left by the structural components during the manufacturing process will directly affect the structural rigidity, stable bearing capacity, corrosion resistance, deformation resistance, and fatigue strength of the welded components, which often leads to delayed cracking or cracks in the welded structural components, affecting the strength of the structure, the safety, and reliability of steel structures [1–4]. Relevant scholars have conducted relevant research on their distribution and measurement. C. Pandey et al. studied the effects of different welding directions on the geometric shape of welds, established the limited element (Fe) model of the two-sided angle welding of buried arc welding, and used the test results to verify the simulation results [5]. P.K. Taraphdar et al. established different finite element models to study its ability to predict the accuracy of the residual stress distribution of welded seam section, and verify its analysis results [6]. Sun et al. measured the residual stress of the S690 high-strength steel welding I-shaped cross-section short pillar through laser cutting and X-ray diffraction technology. The experimental and numerical simulation results show that the impact of residual stress on the structure must be fully considered when designing it. In addition, the effects of high-chromium stainless steel welding processes on the material response and local stability of the I-shaped section were studied, and it was evaluated via experiments and numerical simulation [7,8]. Trayana Tankova et al. researched the residual stress characteristics of welding I-shaped section steel components. The effects of different welding processes, plate thickness and geometric parameters on residual stress distribution were analyzed through experiments and numerical simulation, and their impact on structural performance and design [9]. Lukas Schaper et al. proposed a new residual stress model for welding I-shaped sections. Based on the limited element analysis, the model considers the effects of welding process, plate thickness and geometric parameters on residual stress, and verified the accuracy and reliability of the model through experiments [10].

In order to mitigate the effects of welding-induced residual deformation and residual stress on the performance of structures, various methods are commonly employed, including natural aging, heat treatment, and shock vibration. These techniques aim to weaken or eliminate residual stress. With the development of theoretical research and innovation in production practice, new technology for residual stress elimination is emerging, such as the use of spectral harmonics, pulsed magnetism, electric shock, and ultrasonic shock to eliminate residual stress.

Regardless of the traditional natural aging method, thermal aging method, hammering method, or ultrasonic impact, they all have limitations, and they cannot realize the in situ local regulation and elimination of residual stresses of service components [11–17]. (1) The natural aging method is time-consuming, has low efficiency and a large footprint, and is difficult to control, with other shortcomings limiting its wide and effective application. (2) The thermal aging method has a long cycle, high energy consumption, high economic cost, easy oxidation of the workpiece, serious pollution, and it is difficult to handle large components or heat vulnerable components. (3) The impact method is used to hit the residual stress zone with a hand hammer and a wind hammer to reduce the stress. However, the impact method may bring new defects to the weld and even cause cracking of the weld feet. (4) The vibration method for residual stress relief involves placing the workpiece on an elastic support and applying vibration, typically at the node. Despite its potential benefits, this method faces many obstacles, such as narrow applicability, limited effectiveness, complex operation, and serious noise pollution. (5) The ultrasonic impact method was first proposed by the Paton Welding Institute of the former Soviet Union in 1972, and has been highly valued by experts and scholars in the international welding field and IWE (International Welding Engineers) from then on [18–20]. Najib Ahmad Muhammad et al. researched the effects of Al/MG alloy alien materials ultrasonic auxiliary stirring welding of ultrasonic waves on residual stress and micro-tissue. Experimental and numerical simulation results show that ultrasonic waves can effectively reduce the residual stress at the weld and have an impact on the micro-tissue of the welding area [21]. While the ultrasonic impact is equalizing the residual stress of the in-service components, the surface of the steel component is usually affected by the impact of the horn, which usually causes impact damage or even cracks or micro-cracks. For steel components, these impact damages are prohibited, and will greatly affect the safety and reliability of the bridge structure. Therefore, ultrasonic shock generates new impact or crack damage while eliminating the residual stress of components, which is the biggest problem.

The basic principle of high-energy ultrasound to eliminate residual stress is that the large-amplitude fluctuation of high-energy ultrasound causes the grains or lattices in the area where the residual stress exceeds the standard to produce alternating vibration or creep, and induce a series of secondary effects such as ultrasonic softening and dislocation motion; in addition, the high-energy sound field also produces periodic or intermittent shock waves, which form a local pressure gradient at the wavefront, thereby causing local heating of the grain boundary, and accelerating the softening of the material, promoting the slip between the grains, and finally eliminating the residual stress. The new elimination technology has the advantages of having a good stress relief effect, low cost, low energy consumption, high speed, being easy to use in the field of mechanical workpiece service, and can realize in situ local focusing control, among others.

In this paper, on the basis of detecting residual stress with ultrasonic critical refraction longitudinal wave, after finding out the position of welding residual stress on the upper chord of the main truss of Sanguantang steel truss bridge, high-energy ultrasonic equipment is used to eliminate the residual stress.

The results indicate that the high-energy ultrasonic method achieves an overall elimination rate of welding residual stress ranging from 24.52% to 37.23%, with more significant reduction effects observed in areas with higher initial residual stress levels. These findings demonstrate that the high-energy ultrasonic method is a reliable and effective approach for residual stress elimination, supported by the scientific and efficient performance of the high-energy ultrasonic residual stress elimination equipment.

2. Principle of Eliminating Residual Stress via High Energy Ultrasonic Method

2.1. Strain Energy Density

The energy density equation is [22–24]

$$A = A(F, F^P, \varepsilon^P, \theta^P, T, E_u) \quad (1)$$

Decompose the free energy density Equation (1) into elastic and plastic parts [25,26]:

$$A = A(F, F^P, \varepsilon^P, \theta^P, T, E_u) = W^e(FF^P, T) + W^P(\varepsilon^P, \theta^P, T, E_u) \quad (2)$$

where F is the deformation gradient, F^P is the plastic part of the deformation gradient, ε^P is the effective partial plastic strain, θ^P is the effective bulk plastic strain, the absolute temperature T/°C, and the rate of ultrasonic energy per unit area, which is the ultrasonic intensity/(W·m^{-2}).

Where the superscript represent the elastic and plastic parts of the respective variable functions, respectively.

The elastic strain energy density is defined as follows:

$$W^e(\varepsilon^e, T) = W^{e,vol}(\theta^e, T) + W^{e,dev}(e^e, T) \quad (3)$$

$$W^{e,vol}(\theta^e, T) = \frac{E_k}{2}[\theta^e - \alpha_r(T - T_0)]^2 + \rho_0 C_v T(1 - \log\frac{T}{T_0}) \quad (4)$$

$$W^{e,\mathrm{dev}}(e^e, T) = G\|\mathrm{dev}(\varepsilon^e)\|^2 \quad (5)$$

where, $\theta^e = \log J^e$, G is the shear modulus/MPa, α_r is the coefficient of thermal expansion/°C^{-1}, T_0 is the reference absolute temperature/°C, C_v is the constant volume specific heat per unit mass/(J·kg^{-1}·K^{-1}). Similar to the elastic strain energy density, the plastic stored energy is also assumed to be the sum of the volume and deviator. The deviatoric part is defined as a regular power law, while the bulk part is the sum of the plastic energy stored in each individual void using the following relation:

$$W^P(\varepsilon^P, \theta^P, T, E_u) = W^{P,vol}(\theta^P, T, E_u) + W^{P,dev}(e^P, T, E_u) \quad (6)$$

$$W^{P,dev}(e^P, T, E_u) = \frac{\eta\sigma_0(T, E_u){\varepsilon_0}^P}{\eta + 1}(1 + \frac{\varepsilon^P}{{\varepsilon_0}^P})^{\frac{\eta+1}{\eta}} \quad (7)$$

$$W^{P,vol}(\theta^P, T, E_u) = \frac{\eta\sigma_0(T, E_u){\varepsilon_0}^P}{\eta + 1} N_V \frac{4\pi a^3}{3} g(\theta^P, \eta) \quad (8)$$

where

$$g(\theta^P,\eta) = \int_1^{1/f}\left(1+\frac{2}{3\varepsilon_0^p}\log\frac{x}{x-1+\frac{f_0}{f_0+\exp\theta^p-1}}\right)^{\frac{\eta}{\eta+1}}dx \tag{9}$$

where η is the hardening exponent, $\sigma_0(T)$ is the yield stress/MPa at temperature T, and ε_0^P is the reference partial plastic strain.

According to the basic assumptions for acoustic softening of different materials, the relationship between yield stress and thermal and acoustic softening effects is as follows [27,28]:

$$\sigma_0(T) = \sigma_0(T_0)\left(1-\frac{T-T_0}{T_m}\right)^{\psi}(1-\mathrm{d}\cdot E_\mathrm{u})^{e} \tag{10}$$

where T_0 is the reference temperature/°C, T_m is the melting temperature/°C, and c is the softening index. Ultrasonic intensity E_u (the rate of ultrasonic energy passing through a unit area)/(W·m^{-2}) is defined as follows:

$$E_\mathrm{u} = \frac{\sigma_a^2}{\rho V} \tag{11}$$

Here the acoustic stress, $\sigma_a = \rho V_\mathrm{x}\cdot V$, V_x is the velocity of a specific particle/(m·s^{-1}), and V is the velocity of the ultrasound in the medium/(m·s^{-1}). The velocity at each point of the material during each increment is used to calculate the acoustic stress and the rate of ultrasonic energy per unit area.

2.2. Strain Energy Density

Summarize the incremental solution process used in constitutive equations, time discretized as t_n (past) and t_{n+1} (present). Assuming that the state of the material $\left(F^P,\xi_n^P,\theta_n^P,\dot{\theta}_n^P,\ddot{\theta}_n^P\right)$ is known, the deformation gradient F_{n+1}, temperature T_{n+1}, and high-energy ultrasound intensity are known to the constitutive model for the moment $E_{\mathrm{u},n+1}$. This means that at t_{n+1} time instant, with the direction of incremental plastic deformation M, N, the unknown state variables of the material have $\left(F_{n+1}^P,\xi_{n+1}^P,\theta_{n+1}^P,\dot{\theta}_{n+1}^P,\ddot{\theta}_{n+1}^P\right)$. At this point, there is [29]:

$$W_n\left(F_{n+1},T_{n+1},E_{\mathrm{u},n+1}\right) = \min_{\xi_{n+1}^P,\theta_{n+1}^P,M,N} f_n\left(F_{n+1},T_{n+1},E_{\mathrm{u},n+1},\xi_{n+1}^P,\theta_{n+1}^P,M,N\right) \tag{12}$$

The minimum value of the above variational form returns the correction value when the unknown state variables and plastic flow direction are returned. The above minimum value at t_{n+1} time instant is the effective incremental strain energy density, which can act as the Piola-most Kirchhoff stress tensor of the first kind P_{n+1}. The tangential modulus DP_{n+1} is obtained from the linearization of the equation $P = \frac{\partial A}{\partial F}$. The incremental variational problem is solved according to the predicted correction method of the logarithmic elastic strain, thereby reducing the finite deformation, and the correction is small strain and pure dynamic [30].

Two methods of software simulation and experimental testing are used to verify the correctness of the theory. The first group of experiments used Q235 ordinary carbon structural steel tensile test, and the mechanical properties of the experimental materials are shown in Table 1. The same parameters were used for the experiment and simulation, that is, the shear rate was constant 5 mm/min with and without ultrasonic energy. The high-energy ultrasonic power is 250 W, and the frequency is 20 KHz. The first set of experimental results, shown in Figure 1, was performed using the uniaxial tensile experimental data of Daud et al. The simulation results are in good agreement with the experimental results.

Table 1. Q235 and Q345 mechanical properties [31].

Material	Yield Strength/MPa	Tensile/MPa	Density/(kg·m^{-3})	Elongation/MPa
Q235	≥235	≥370	7850	≥21
Q345	≥345	≥490	7850	≥22

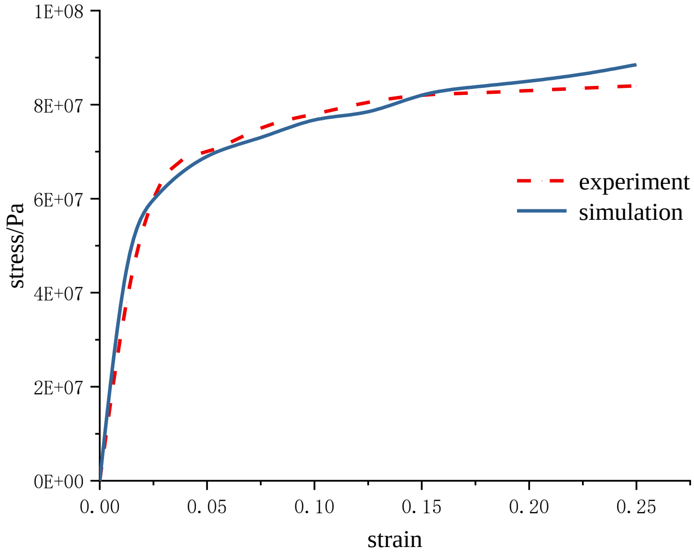

Figure 1. Comparison of constitutive model and experimental data without ultrasonic energy.

The second set of experiments used Q345 steel, and the mechanical properties of the material are shown in Table 1. The same high-energy ultrasonic excitation was used as in Experiment 1, except that the high-energy ultrasonic generator was turned on and then turned off. The experimental results are shown in Figure 2, using the experimental data of Siddiq et al. The experimental results show the following: when the ultrasonic generator is turned on, the stress required to generate the same strain decreases immediately, which is due to the ultrasonic softening effect; when the ultrasonic generator is turned off, the tensile stress rebounds to a higher value than the average value. This phenomenon is akin to work hardening and is independent of the frequency of the high-energy ultrasonic waves; rather, it is correlated with the intensity of the waves.

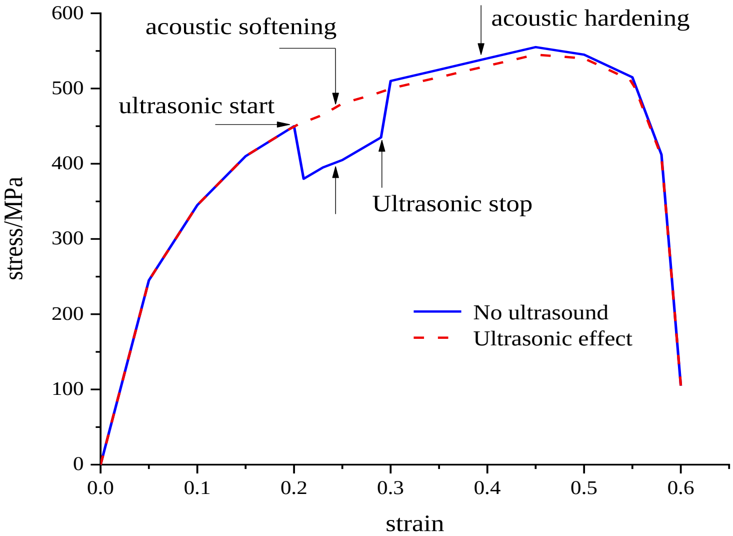

Figure 2. Comparison of test data before and after the application of Q345 ultrasonic energy.

It can be observed that the softening effect occurs when a material undergoes elastic or plastic deformation and is exposed to high-energy ultrasonic energy. This leads to a significant decrease in the yield strength and tensile strength of the material. After high-energy ultrasonic removal, the tensile strength returned to its initial value and some work hardening occurred. The effect of high-energy ultrasound on metals is somewhat similar to that of heat treatment; however, the efficiency of high-energy ultrasound is extremely high. For example, for aluminum alloy materials, it only takes one ten millionth of the energy to produce the same softening effect as heat treatment. Not only that, other metals such as iron, copper and other materials will soften under the radiation effect of high-energy ultrasonic sound field.

3. High-Energy Ultrasonic Method to Eliminate Residual Stress System

3.1. Technical Indicators of High-Energy Ultrasonic Elimination System

Compared with the technical indicators of other residual stress relief methods at home and abroad, such as heat treatment, ultrasonic shock, vibration aging, etc., the technical indicators of the high-energy ultrasonic relief system are formulated according to the characteristics of the project, as shown in Table 2.

Table 2. Main technical indicators of residual stress high-energy ultrasonic elimination equipment.

Function	Index
Regulate Elimination	Common materials such as carbon steel, low alloy steel, aluminum, etc.
Regulated Elimination/KHz	15~21
Regulated Elimination/W	Single high-energy ultrasonic transducer ≥100
Stress Relief Rate	One-time regulation ≥30%
Single-point control elimination time	≤30 min

3.2. Composition of High-Energy Ultrasonic Elimination System

The residual stress relief system includes high-energy ultrasonic generator, high-energy ultrasonic exciter, and peripheral equipment (including transducer vacuum/magnetic clamping device, excitation voltage transmission cable, couplant, etc.). The system block diagram is shown in Figure 3.

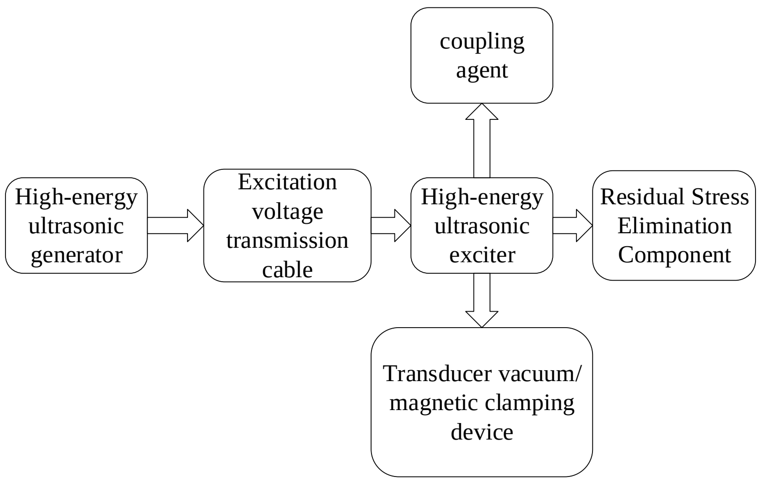

Figure 3. Diagram of the residual stress high-energy ultrasonic elimination system.

4. Application of High-Energy Ultrasonic Method to Eliminate Residual Stress

4.1. Engineering Introduction

The Sanguantang bridge (as shown in Figure 4) and its connection project are located in the east of Ningbo City. It is the main crossing in Jiangtong, connecting the Academician Road of the High-tech Zone and Zhenhaiming Avenue. It starts from the Jiang Road that has been built in the high-tech zone in the south, and connects with the existing high-tech zone in the south of Zhenhai. The Jiang Road in the north is connected to the west of the current state of Zhenhai in the north. The total length of the route is 3300 m, crossing the Yongjiang River and four planned rivers. The bridge project mainly includes the main bridge spanning the Yongjiang River, the connecting approach bridge on the south bank of the Yongjiang River, the connecting approach bridge on the north bank and the ground bridge. The total length of the main bridge is 2203 m.

Figure 4. Sanguantang bridge [32].

The welding seam of the upper chord of the main truss of the steel truss girder of the Sanguantang bridge is dense, and the welding quality is directly related to the safety of the bridge structure. In the process of welding residual stress detection, it is found that the stress in the local area is too large, and it is necessary to carry out welding stress relief work.

4.2. Residual Stress Relief Point Layout Principle

The high-energy ultrasonic method selects the area of stress relief points based on the results of ultrasonic stress testing. The selection principles for stress relief points are as follows:

(1) The ultrasonic stress test results show that there is obvious stress concentration in a certain area;
(2) When the tensile stress value is greater than or equal to half of the yield strength of the material (for example, the yield strength of Q420qE is about 420 Mpa, when the test result is greater than or equal to 210 Mpa, stress regulation and elimination are required);
(3) When the tensile stress value is greater than or equal to the allowable stress value of the tested material;
(4) When it is greater than the stress value agreed upon by the designer or the builder.

4.3. Layout of Residual Stress Relief Points

The residual stress detection sections of the upper chord butt weld of the main truss of the steel truss girder bridge are 17#,18#,19#,20# sections on the north bank and 18#,19#,20# sections on the south bank. After the stress detection of the butt welds of the above-mentioned segment roofs, the stress-relief treatment was carried out by selecting the areas with greater stress according to the stress detection results and using the high-energy ultrasonic method. For the segment that needs stress relief, the stress relief point is at the same position as the weld stress detection point. Taking 18# weld as an example, the measuring point layout is shown in Figure 5.

The inspection shows that the butt welds of the upper chord on the left and right sides of the 18# segment on the south bank of the steel truss girder bridge, the butt weld of the upper chord on the left side of the 20# segment on the south bank, the butt weld of the upper chord on the right side of the 18# segment on the north bank and the 19# on the north bank. The residual stress value of the butt weld of the upper chord on the right side of the segment is too large; therefore, the high-energy ultrasonic method is used to eliminate the welding residual stress.

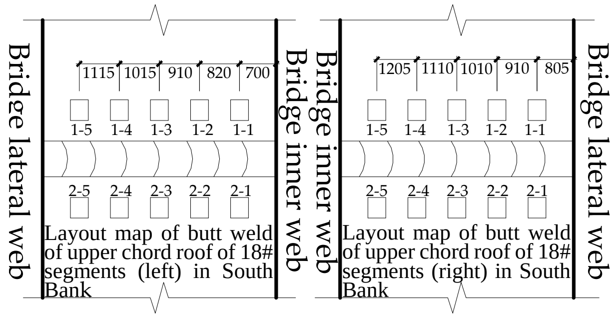

Figure 5. Arrangement of stress measurement points for the butt welds of the top chord roof of the main truss of the 18# segment of the South Bank. (The direction is based on north to south).

4.4. Field Operation of High-Energy Ultrasound to Eliminate Residual Stress

The transducers in the high-energy ultrasound equipment are shown in Figure 6. Figure 7 shows the field operation diagram of high-energy ultrasonic to eliminate residual stress.

Figure 6. High-energy ultrasonic transducer and tooling diagram.

Figure 7. Field operation diagram of high-energy ultrasonic to eliminate residual stress.

During the elimination process, the exciter wedge should be firmly and tightly attached to the surface of the material, and the coupling contact force should remain stable during the control process. The specific operation of the elimination process is as follows:

(1) The electrical connection of the working system is intact and meets the specifications and requirements of the equipment;
(2) Place the exciter on the surface of the material according to the required control mode, apply the coupler evenly on the end face of the exciter, and clamp the exciter on the surface of the component stably by vacuum, magnetic attraction or mechanical clamping to ensure that the end face of the exciter and the surface curvature of the components are fitted and tightly coupled;

(3) After checking that the connection of the working system is correct, turn on the system equipment and start working, set the exciter to work at the natural frequency, and adjust the optimum frequency and working time of the exciter according to the pressing state of the tooling and the excitation effect, so that the exciter can work properly and is maintained in the best working condition;
(4) After the residual stress elimination process is over, close the elimination equipment, remove the clamping tool, and clean the surface of the component and the end face of the sound beam exciter coupler;
(5) Record the process parameters.

In the process of residual stress elimination, if it is found that the residual stress changes before and after elimination are small. In addition, it should be considered whether the curvature of the excitation wedge and the surface of the component fit, whether the coupling is good, whether the exciter works normally, and whether the power supply and the output power of the exciter are sufficient. If it is caused by other factors, it can be re-controlled after correction.

5. Analysis of the Results of High-Energy Ultrasound to Eliminate Residual Stress

After inspection, it was found that the butt welds of the upper chord on the left and right sides of the 18# section in the south bank, the butt welds of the upper chord on the right side of the 18# section in the north bank, the butt weld of the upper chord on the right side of the 19# section in the north bank, and the left side of the 20# section in the south bank. The welding residual stress value of the butt weld of the upper chord is too large, and the above area needs to be eliminated using a high-energy ultrasonic method. According to the comparison of the data before and after the welding residual stress is eliminated in Tables 3–5, it can be seen that the high-energy ultrasonic method can effectively eliminate the welding residual stress. The overall welding residual stress elimination rate this time is 24.52% to 37.23%; more obvious. See Tables 3–7 for the elimination effect, and Figures 8–12.

Table 3. Comparison before and after the welding residual stress of the upper chord on the left side of the 18# segment of the south bank.

Measuring	Before Stress	After Stress	Stress Relief
1-1	197.80	127.33	35.62%
1-2	137.24	92.03	32.94%
1-3	168.42	120.36	28.54%
1-4	126.13	66.43	47.33%
1-5	134.49	92.55	31.19%
2-1	170.33	114.88	32.55%
2-2	141.18	87.20	38.24%
2-3	124.70	85.33	31.57%
2-4	182.04	108.69	40.29%
2-5	142.98	102.21	28.51%
average	152.53	99.70	34.68%

Table 4. Comparison before and after the welding residual stress of the upper chord on the right side of the 18# segment of the south bank.

Measuring	Before Stress	After Stress	Stress Relief
1-1	140.47	68.42	51.29%
1-2	186.34	121.57	34.76%
1-3	187.29	109.41	41.58%
1-4	77.16	62.20	19.39%
1-5	158.39	103.34	34.75%
2-1	139.57	86.89	37.75%

Table 4. *Cont.*

Measuring	Before Stress	After Stress	Stress Relief
2-2	117.94	92.46	21.61%
2-3	85.59	77.67	9.25%
2-4	133.30	101.53	23.83%
2-5	144.20	103.36	28.32%
average	137.02	92.69	30.25%

Table 5. Comparison before and after the welding residual stress of the upper chord on the right side of the 18# segment of the north bank.

Measuring	Before Stress	After Stress	Stress Relief
1-1	137.36	92.11	32.94%
1-2	182.38	106.64	41.53%
1-3	77.16	78.22	−1.37%
1-4	124.70	76.33	38.79%
1-5	94.36	80.15	15.06%
2-1	173.79	108.47	37.59%
2-2	152.96	96.66	36.81%
2-3	84.57	77.38	8.50%
2-4	79.79	72.64	8.96%
2-5	82.42	60.68	26.37%
average	118.95	84.93	24.52%

Table 6. Comparison before and after the welding residual stress of the upper chord on the right side of the 19# segment of the north bank.

Measuring	Before Stress	After Stress	Stress Relief
1-1	47.66	17.20	63.91%
1-2	136.17	70.00	48.60%
1-3	178.35	136.78	23.31%
1-4	137.24	83.67	39.04%
1-5	203.53	82.18	59.62%
2-1	120.11	99.56	17.11%
2-2	107.86	106.07	1.66%
2-3	79.19	65.27	17.58%
2-4	99.47	78.36	21.22%
2-5	115.38	100.05	13.29%
average	122.50	83.91	30.53%

Table 7. Comparison before and after the welding residual stress of the upper chord on the left side of the 20# segment of the south bank.

Measuring	Before Stress	After Stress	Stress Relief
1-1	140.23	134.12	4.36%
1-2	182.39	97.83	46.37%
1-3	184.42	121.65	34.04%
1-4	187.77	105.11	44.02%
1-5	173.43	78.26	54.88%
2-1	196.37	123.84	36.93%
2-2	115.02	67.08	41.68%
2-3	131.87	48.26	63.41%
2-4	183.76	158.62	13.68%
2-5	215.48	144.41	32.98%
average	171.07	107.92	37.23%

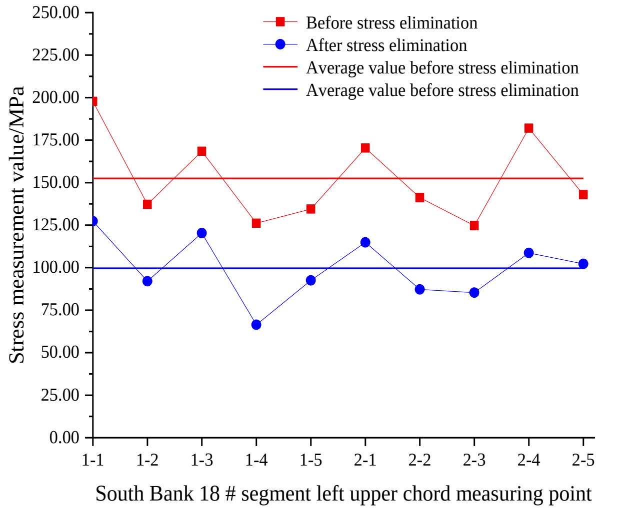

Figure 8. Comparison before and after the welding residual stress of the upper chord on the left side of the 18# segment of the south bank.

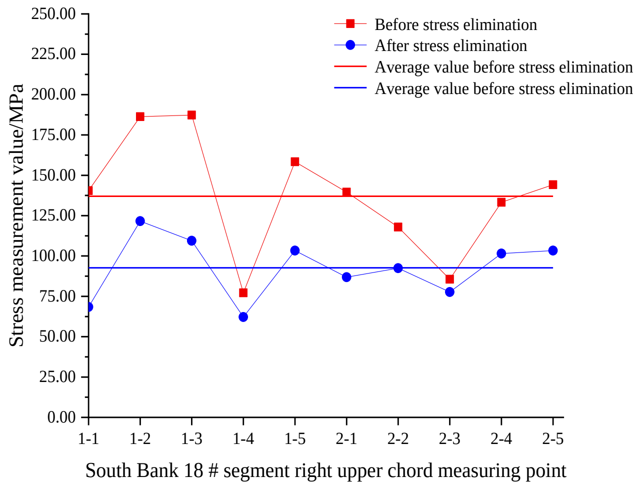

Figure 9. Comparison before and after the welding residual stress of the upper chord on the right side of the 18# segment of the south bank.

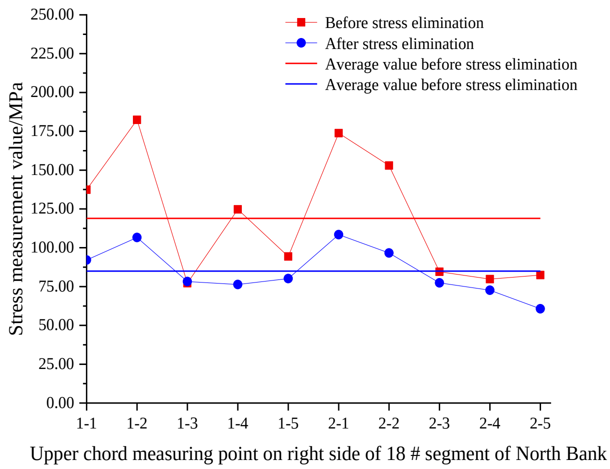

Figure 10. Comparison before and after the welding residual stress of the upper chord on the right side of the 18# segment of the north bank.

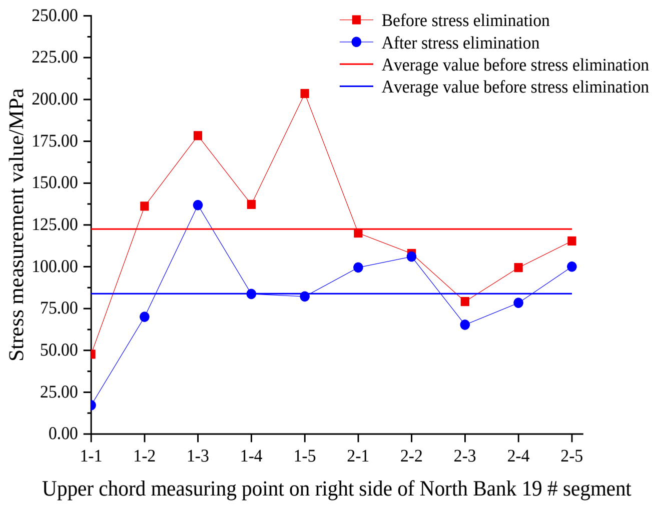

Figure 11. Comparison before and after the welding residual stress of the upper chord on the right side of the 19# segment of the north bank.

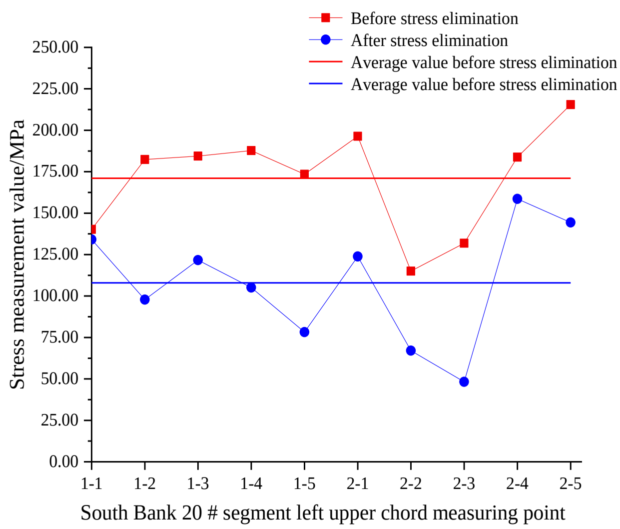

Figure 12. Comparison before and after the welding residual stress of the upper chord on the left side of the 20# segment of the south bank.

6. Conclusions and Recommendations

(1) Field test results demonstrate that residual stress occurs in steel bridge members when welded connections are used, and the stress values are significant, which should be a cause for concern.

(2) Based on the elimination results, the high-energy ultrasonic method is effective in eliminating the welding residual stress of the upper chord of the main truss of the steel truss girder bridge, indicating that this method can be used to eliminate the welding residual stress.

(3) The elimination results show that the overall elimination rate of the welding residual stress is 24.52% to 37.23%, and the reduction effect is more obvious in the zone where the welding residual stress is larger. The reduction in residual stress greatly ensures the safe operation of components.

(4) During the operation of bridge structures, cracking can easily occur under static and dynamic loads. It is recommended to use a remote monitoring system to monitor the welding fatigue of important components. The system uses temperature compensation technology to correct measurement errors and sends measurement results to a remote server. If the measured value exceeds the set range, the server sends an alarm message to notify management personnel.

Author Contributions: Conceptualization, L.P. and J.Y.; methodology, L.P.; validation, N.M., L.P. and R.W.; formal analysis, L.P.; investigation, L.P.; resources, J.Y. and G.Z.; data curation, L.P. and C.Y.; writing—original draft preparation, L.P.; writing—review and editing, N.M., L.P. and R.W.; visualization, L.P. and C.Y.; supervision, L.P., G.Z. and J.Y. All authors have read and agreed to the published version of the manuscript.

Funding: This research was funded by the Natural Science Foundation of Guangdong Province (grant No. 2021A1515012405) and Guangdong Provincial Key Laboratory of Modern Civil Engineering Technology (grant No. 2021B1212040003).

Data Availability Statement: The data presented in this study are available on request from the corresponding author.

Conflicts of Interest: The authors declare no conflict of interest.

References

1. Kleinert, W. *Defect Sizing Using Non-Destructive Ultrasonic Testing*; Springer: Cham, Switzerland, 2016.
2. Büyüköztürk, O.; Taşdemir, M.A. *Nondestructive Testing of Materials and Structures*; Springer: Berlin/Heidelberg, Germany, 2013.
3. Langenberg, K.J.; Marklein, R.; Mayer, K. *Ultrasonic Nondestructive Testing of Materials*; CRC Press: Boca Raton, FL, USA, 2017.
4. Balayssac, J.P.; Garnier, V. *Nondestructive Testing and Evaluation of Civil Engineering*; ISTE Press: London, UK, 2017.
5. Pandey, C.; Giri, A.; Mahapatra, M.M. On the prediction of effect of direction of welding on bead geometry and residual deformation of double-sided fillet welds. *Int. J. Steel Struct.* **2016**, *16*, 333–345. [CrossRef]
6. Taraphdar, P.K.; Kumar, R.; Pandey, C.; Mahapatra, M.M. Significance of Finite Element Models and Solid-State Phase Transformation on the Evaluation of Weld Induced Residual Stresses. *Met. Mater. Int.* **2021**, *27*, 3478–3492. [CrossRef]
7. Sun, Y.; Liang, Y.; Zhao, O. Testing, numerical modelling and design of S690 high strength steel welded I-section stub columns. *J. Constr. Steel Res.* **2019**, *159*, 521–533. [CrossRef]
8. Sun, Y.; Zhao, O. Material response and local stability of high-chromium stainless steel welded I-sections. *Eng. Struct.* **2019**, *178*, 212–226. [CrossRef]
9. Tankova, T.; Da Silva, L.S.; Balakrishnam, M.; Rodrigues, D.; Launert, B.; Pasternak, H.; Tun, T.Y. Residual stresses in welded I section steel members. *Eng. Struct.* **2019**, *197*, 109398. [CrossRef]
10. Schaper, L.; Tankova, T.; Da Silva, L.S.; Knobloch, M. A novel residual stress model for welded I-sections. *J. Constr. Steel Res.* **2022**, *188*, 107017. [CrossRef]
11. Gueudré, C.; Mailhé, J.; Ploix, M.-A.; Corneloup, G.; Chassignole, B. Influence of the uncertainty of elastic constants on the modelling of ultrasound propagation through multi-pass austenitic welds. Impact on non-destructive testing. *Int. J. Press. Vessel. Pip.* **2019**, *171*, 125–136. [CrossRef]
12. Tang, F.D.; Yu, Y.F. Nondestructive testing method for welding quality in key parts of ocean-going ships. *J. Coast. Res.* **2020**, *110*, 91–94. [CrossRef]
13. Rabe, U.; Pudovikov, S. Application of the total focusing method for quantitative nondestructive testing of anisotropic welds with ultrasound. *Tm Tech. Mess.* **2020**, *87*, 438–450. [CrossRef]
14. Deepak, J.; Raja, V.B.; Srikanth, D.; Surendran, H.; Nickolas, M. Non-destructive testing (NDT) techniques for low carbon steel welded joints: A review and experimental study. *Mater. Today Proc.* **2021**, *44*, 3732–3737. [CrossRef]
15. Ke, Q.D.; Li, W.P.; Wang, W.X.; Song, S. Correction method with stress field effects in ultrasound nondestructive testing. *Nondestruct. Test. Eval.* **2022**, *37*, 277–296. [CrossRef]
16. Shaloo, M.; Schnall, M.; Klein, T.; Huber, N.; Reitinger, B. A Review of Non-Destructive Testing (NDT) Techniques for Defect Detection: Application to Fusion Welding and Future Wire Arc Additive Manufacturing Processes. *Materials* **2022**, *15*, 3697. [CrossRef]
17. Milašinović, D.D.; Landović, A.; Goleš, D. Fatigue damage in bending of reinforced concrete frames using non-destructive tests for dynamic strength of the cylinder. *Eng. Comput.* **2022**, *39*, 1534–1555. [CrossRef]
18. Munsi, Y.; Waddell, A.J.; Walker, C.A. The influence of vibratory treatment on the fatigue life of welds: A comparison with thermal stress relief. *Strain* **2008**, *37*, 41–49. [CrossRef]
19. Withers, P.J.; Bhadeshia, H.K.D.H. Residual stress. Part1-Measurement techniques. *Mater. Sci. Technol.* **2001**, *17*, 355–365. [CrossRef]
20. Tang, F.; Lu, A.L.; Mei, J.F.; Fang, H.; Luo, X. Research on residual stress reduction by a low frequency alternating magnetic field. *J. Mater. Process. Technol.* **1998**, *74*, 255–258. [CrossRef]
21. Muhammad, N.A.; Geng, P.; Wu, C.; Ma, S. Unravelling the ultrasonic effect on residual stress and microstructure in dissimilar ultrasonic-assisted friction stir welding of Al/Mg alloys. *Int. J. Mach. Tools Manuf.* **2023**, *186*, 104004. [CrossRef]
22. Kong, C.Y.; Soar, R.C.; Dickens, P.M. A model for weld strength in ultrasonically consolidated components. *Proc. Inst. Mech. Eng. Part C J. Mech. Eng. Sci.* **2005**, *29*, 83–91. [CrossRef]
23. Kong, C.Y.; Soar, R.C.; Dickens, P.M. Optimum process parameters for ultrasonic consolidation of 3003 aluminum. *J. Mater. Process. Technol.* **2004**, *146*, 181–187. [CrossRef]

24. Lucas, M.; Daud, Y. A finite element model of ultrasonic extrusion. In Proceedings of the 7th International Conference on Modern Practice in Stress and Vibration Analysis, Cambridge, UK, 8–10 September 2009; pp. 181–189.
25. Siddiq, A.; Sayed, T.E. Acoustic softening in metals during ultrasonic assisted deformation via CP-FEM. *Mater. Lett.* **2011**, *65*, 356–359. [CrossRef]
26. Siddiq, A.; Sayed, T.E. A thermomechanical crystal plasticity constitutive model for ultrasonic consolidation. *Comput. Mater. Sci.* **2012**, *51*, 241–251. [CrossRef]
27. Susan, M.; Munteanu, C. On the drawing in-ultrasonic field of metallic wires with high mechanical resistance. *J. Optoelectron. Adv. Mater.* **2005**, *7*, 637–645.
28. Weinberg, K.; Mota, A.; Ortiz, M. A variational constitutive model for porous metal plasticity. *Comput. Mech.* **2006**, *37*, 142–152. [CrossRef]
29. Zhu, Z.; Wynne, B.P.; Ghassemieh, E.; Siddiq, M.A. Microstructural analysis of ultrasonic welded AA6061 by electron backscattered diffraction. *Rare Met. Mater. Eng.* **2009**, *38*, 147–151.
30. Daud, Y.; Lucas, M.; Huang, Z. Ultrasonic compression tests on aluminum. *Appl. Mech. Mater.* **2005**, *4*, 99–104.
31. *GB/T 1591-2008*; High Strength Low Alloy Structural Steel. China Standards Press: Beijing, China, 2008.
32. A Cross-River Bridge under Construction in Zhejiang Province, with a Main Span of 465 Meters and a Total Length of 3.3 Kilometers, Sets a New Record in China. Available online: https://m.sohu.com/a/312861340_100250366?strategyid=00014 (accessed on 9 May 2019).